2011 American Control Conference
on O'Farrell Street, San Francisco, CA, USA
June 29 - July 01, 2011

Model Predictive Control of Trailing Edge Flaps on a Wind Turbine blade

Damien Castaignet, Niels K. Poulsen, Thomas Buhl and Jens Jakob Wedel-Heinen

Abstract— **Trailing Edge Flaps on wind turbine blades have been studied in order to achieve fatigue load reduction on the turbine components. We show in this paper how Model Predictive Control can be used to do frequency weighted control of the trailing edge flaps in order to reduce fatigue damage on the blade root. The design model is based on a modal model of the blade structure and a steady state aerodynamic model of the blade airfoils. Depending on the output filter, loads within different frequency range are decreased. A fine tuning of the Kalman filter and of the cost function allows to decrease significantly the blade root loads without damaging excessively the trailing edge flap actuators.**

I. Introduction

Wind turbines rotor size has increased significantly over the last years in order to harvest more energy and to reduce the cost of wind energy. A large part of modern wind turbines have now blades longer than 40 m. This increase in blades size results in an increase in both fatigue and extreme loads in the main components of the turbine: blades, drive train, tower, foundations etc. Decreasing those loads is important in order to keep the cost of energy low.

Some modern Megawatt size turbines use cyclic pitch or individual pitch control in order to alleviate some of these loads [1], [2]. Larsen et al. [1] showed that blade flap fatigue loads can be reduced by 28% using individual pitch control. Since 2003, Trailing Edge Flaps (TEF) have been studied as a possible way to alleviate even more loads [3], [4]. Those actuators have the advantage of controlling the flow locally, where it has the most impact on the loads [5]. They can also be actuated at a higher frequency than the pitch system. Wind tunnel experiments on a 2D section of a blade equipped with active trailing edge flaps [6], [7] and on a scaled rotating two-bladed smart rotor [8] confirm their potential . At last, a full scale test was carried out on a Vestas V27 turbine at Risø DTU [9].

Several control strategies have been investigated. Lackner et al. designed a PID Individual Flap Control based on the Individual Pitch Control scheme, using the Coleman transformation to make the system linear time invariant [10]. Van Wingerden et al. used subspace system identification to fine tune the PD controller used in their wind tunnel test [7]. Rice et al. focused on a robust and distributed control in order to ensure stability of the controller despite non linearities and model mismatch [11]. At last, Wilson et al. designed PD feedback controllers based on tip deflection or tip deflection rate, and showed a decrease in the standard deviation of the root flap bending moments [12].

This work is part of the ATEF project, which is partially funded by Danish National Advanced Technology Foundation (Højteknologifonden)

D. Castaignet and J.J. Wedel-Heinen are with Vestas Wind Systems A/S, Global Research, Roskilde, Denmark daca@vestas.com

N. K. Poulsen is with the Technical University of Denmark, DTU Informatics, Lyngby, Denmark

T. Buhl is with Risø DTU, National Laboratory for Sustainable Energy, Roskilde, Denmark

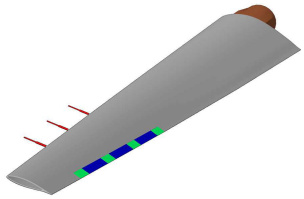

Fig. 1. Illustration of the Vestas V27 blade equipped with trailing edge flaps (blue) and Pitot tubes (red).

This paper shows the design of a Model Predictive Control (MPC) in order to do frequency weighted control on the blade root flap bending moment variations. The system is based on the experimental V27 turbine located at Risø DTU and equipped with 3 independent trailing edge flaps [9].

II. Model/System

A. System

The Vestas V27 turbine is a pitch controlled horizontal axis wind turbine, with a nominal power of 225kW, and 13 meter long blades. The model predictive control described in this paper is meant to be tested in the future on the V27 turbine located at Risø DTU, National Laboratory for Sustainable Energy, Roskilde, Denmark. The turbine has been equipped with trailing edge flaps and extra sensors for the purpose of the ATEF project. One of the 3 blades is equipped with 3 independent trailing edge flaps (Fig. 1). Among the sensors available for this experiment are 3 Pitot tubes at the leading edge of the blade, and strain gages at the blade root [9].

The pitch control of the V27 turbine is unchanged. The controller described in this paper only actuates the trailing edge flaps. It aims at decreasing the blade root fatigue loads, while the pitch controller regulates the power production.

The configuration of actuators and sensors used in this paper matches the experimental blade available within this project.

B. Non-linear model

The design model of the model predictive control includes only the structural and the aerodynamic model of the blade. This model is based on the non-linear aero-elastic model of

a wind turbine developed at DTU Mechanical Engineering and implemented in the aero-elastic code Flex [13].

1) Structural model: The blade structure is modeled by its mode shapes. It takes into account the blade deflection in 2 directions: flapwise and edgewise. If the N_g first mode shapes of the blade are considered, then the flapwise and edgewise deflections of the blade section x at time t, respectively $u_z(x,t)$ and $u_y(x,t)$, are:

$$u_z(x,t) := \sum_{i=1}^{N_g} g_i(t) u_z^i(x),\ u_y(x,t) := \sum_{i=1}^{N_g} g_i(t) u_y^i(x),$$

$u_z^i(x)$ and $u_y^i(x)$ are respectively the flapwise and edgewise deflection of the blade section x under mode shape i. $g_i(t)$ are the generalised coordinates associated to mode shape i. A generalised mass M_{g_i}, stiffness K_{g_i} and damping C_{g_i} are associated to each of the mode shapes. The torsion mode of the blade is neglected in this model due to the high torsion stiffness of the V27 blade.

Newton's second law applies to each of the generalised modes: $M_{g_i}\ddot{g_i} + C_{g_i}\dot{g_i} + K_{g_i}g_i = F_{g_i}$. F_{g_i}, the generalised force for mode shape i, is the work done by the external loads (aerodynamic, centrifugal and gravity loads) on this mode shape: $F_{g_i} = \int p_z(x)u_z^i(x)dx + \int p_y(x)u_y^i(x)dx$, where $p_z(x)$ and $p_y(x)$ are the external loads, respectively flapwise and edgewise, acting on blade section x.

2) Aerodynamic model: The aerodynamic forces on an airfoil with a trailing edge flap depend on the local wind speed $\mathbf{V_r}(x,t)$, the local angle of attack $\alpha(x,t)$ and the trailing edge flap angle $\beta(x,t)$. The relative wind speed $\mathbf{V_r}(x,t)$ seen by the airfoil is calculated as $\mathbf{V_r}(x,t) := \mathbf{V_0}(x,t) + \mathbf{W}(x,t) - \mathbf{V_b}(x,t)$, where $\mathbf{V_0}$ is the free wind speed, $\mathbf{W}$ the induced velocities and $\mathbf{V_b}$ the blade velocity. The induced velocities depend on the thrust generated on the rotor by the aerodynamic forces. They are derived from the unsteady Blade Element Momentum [13].

At last, a dynamic stall model is used in order to derive the dynamic lift and drag dynamic coefficients, C_L and C_D, of the airfoil with a given angle of attack α, a trailing edge flap angle β and a relative wind speed $\mathbf{V_r}$. The dynamic stall model used in this paper is the one derived by Andersen and al. [14]. The flapwise and edgewise aerodynamic loads, $p_z^{aero}(x)$ and $p_y^{aero}(x)$, are derived from the lift and drag coefficients:

$$p_z^{aero}(x) := \frac{1}{2}\rho|\mathbf{V}_r|^2 C(x)\left(C_L(x)\cos(\alpha) + C_D(x)\sin(\alpha)\right),$$
$$p_y^{aero}(x) := \frac{1}{2}\rho|\mathbf{V}_r|^2 C(x)\left(-C_L(x)\sin(\alpha) + C_D(x)\cos(\alpha)\right),$$

where ρ is the air density, and $C(x)$ the airfoil chord length.

3) Differential equations: Finally, the system of differential equations modeling the blade structure is, for each mode shape j:

$$M_{g_j}\ddot{g}_j + C_{g_j}\dot{g}_j + K_{g_j}g_j = F_{g_j}(g_i, \dot{g}_i, \omega, \varphi, \mathbf{V}_0, \mathbf{W}, \beta_j). \quad (1)$$

The differential equations relative to the dynamic stall model and the induced velocities can be found in [14] and [13].

4) Blade root moment: The flap blade root moment, measured by a strain gage, is $M_{z5} := EI\frac{\partial^2 u_z(x,t)}{\partial x^2}$, where E is the blade root's modulus of elasticity, flapwise, and I its moment of inertia.

C. Linear model

Some simplifications are made on the non-linear model previously described before it is linearised.

- Only the first mode of the blade (dominated by flapwise deflections) is taken into account. The V27 blade is small and stiff, and simulations and measurements show that the second mode is hardly excited.
- The rotor speed is considered constant; the Vestas V27 turbine generator is fixed speed.
- Aerodynamic lags are also neglected. The Vestas V27 is a pitch controlled wind turbine. In normal production, the flow around the airfoils stays attached and aerodynamic lags are then negligible.
- Induced velocities, which have a slow dynamic, are considered constant.
- Relative wind speeds $\mathbf{V}_r(x,t)$ can not be measured at each point of the blade. 3 Pitot tubes along the blade measure the local wind speeds in the airfoil plan. Those measurements $\mathbf{V_P}$ are interpolated along the blade.

The system of differential equations (1) is simplified and linearised at a given steady-state point. The upperscript ^{0} refers to the steady-state point values and tilded variables are the difference between a variable and its steady-state value: $\tilde{F_{g_i}} = F_{g_i} - F_{g_i}^0$. β is the vector of the TEF angles. $\nabla_x = \frac{\partial \tilde{F}_{g_1}}{\partial x}$ are the gradients of the generalised force for mode shape 1. The linearised generalised force for the first mode shape is then:

$$\tilde{F}_{g_1} = \nabla_{\tilde{g}_1}\tilde{g}_1 + \nabla_{\dot{\tilde{g}}_1}\dot{\tilde{g}}_1 + \nabla_{\tilde{\varphi}}\tilde{\varphi} + \nabla_{\tilde{\beta}}\tilde{\beta} + \nabla_{\tilde{\mathbf{V}}_\mathbf{P}}\tilde{\mathbf{V}}_\mathbf{P}.$$

The differential equation (1) becomes

$$M_{g_1}\ddot{\tilde{g}}_1 + C_{g_1}\dot{\tilde{g}}_1 + K_{g_1}\tilde{g}_1 = \nabla_{g_1}\tilde{g}_1 + \nabla_{\dot{\tilde{g}}_1}\dot{\tilde{g}}_1 + \nabla_{\tilde{\varphi}}\tilde{\varphi} + \nabla_{\tilde{\beta}}\tilde{\beta} + \nabla_{\tilde{\mathbf{V}}_\mathbf{P}}\tilde{\mathbf{V}}_\mathbf{P},$$

and the blade root flap moment $\tilde{M}_f = EI\frac{\partial^2 u_z^1(x)}{\partial x^2}\tilde{g}_1$. Written as a state-space form, the blade model is:

$$\dot{\mathbf{x}} = \mathbb{A}\mathbf{x} + \mathbb{B}\mathbf{u} + \mathbb{G}\mathbf{d},\ \mathbf{y} = \mathbb{C}\mathbf{x},\ \mathbf{z} = \mathbb{C}_m\mathbf{x}, \quad (2)$$

where the state vector $\mathbf{x} := \begin{pmatrix} \tilde{g}_1 \\ \dot{\tilde{g}}_1 \end{pmatrix}$, the input vector $\mathbf{u} := \tilde{\beta}$, the measured disturbance vector $\mathbf{d} := \begin{pmatrix} \tilde{\varphi} \\ \tilde{\mathbf{V}}_\mathbf{P} \end{pmatrix}$, the output vector $\mathbf{y} := \left(\tilde{M}_f\right)$, the measurement vector $\mathbf{z} := \left(\tilde{M}_f\right)$ and the state space matrices are

$$\mathbb{A} := \begin{bmatrix} 0 & 1 \\ M_{g_1}^{-1}\left(\nabla_{\tilde{g}_1} - K_{g_1}\right) & M_{g_1}^{-1}\left(\nabla_{\dot{\tilde{g}}_1} - C_{g_1}\right) \end{bmatrix}, \quad (3)$$

$$\mathbb{B} := M_{g_1}^{-1}\nabla_{\tilde{\beta}}, \quad (4)$$

$$\mathbb{G} := \begin{bmatrix} M_{g_1}^{-1}\nabla_{\tilde{\varphi}} & M_{g_1}^{-1}\nabla_{\tilde{\mathbf{V}}_\mathbf{P}} \end{bmatrix}, \quad (5)$$

$$\mathbb{C} := \mathbb{C}_m = \begin{bmatrix} EI\frac{\partial^2 u_z^1(x)}{\partial x^2} & 0 \end{bmatrix}. \quad (6)$$

This system is both observable and controllable.

III. Model predictive control

A. Objective

The controller's objective is to reduce the fatigue loads at the blade root, or in other terms, to maximise the life time of the blade root. The fatigue damage of a blade is estimated by the equivalent number of cycles it has been through. The calculation of this equivalent number of cycles is based on the Rainflow counting of the loads history and the Wöhler curve of the material. This method can not be used to design the Model Predictive Control. But [15] showed the relation between the fatigue damage and the spectral properties of the loads. The controller's objective is then to reduce the amplitude of the blade root moment variations at given frequencies.

B. Model

The linearized system (2) is, for the purpose of control design, discretized at the sampling frequency (50 Hz). In order to handle uncertainties and disturbances, the model is augmented with noise terms. It is assumed that both the process ($\mathbf{w}_k$) and the measurement noise (ν_k) are sequences of zero mean, Gaussian white noise: $\mathbf{w}_k \in \mathcal{N}(0, R_1)$ and $\nu_k \in \mathcal{N}(0, R_2)$.

$$\begin{aligned}\mathbf{x}_{k+1} =&\mathbb{A}^d\mathbf{x}_k + \mathbb{B}^d\mathbf{u}_k + \mathbb{G}^d\mathbf{d}_k + \mathbf{w}_k,\\ \mathbf{y}_k =&\mathbb{C}^d\mathbf{x}_k,\ \mathbf{z}_k = \mathbb{C}^d_m\mathbf{x}_k + \nu_k\end{aligned}$$

The aero-elastic code Flex uses the same modal approach as the linear model of the blade described previously. So the covariances R_1 and R_2 can be estimated by comparing the model output with simulation results with same inputs. Those covariances can then be tuned by running simulations with different values.

Basically we will control the trailing edge flaps in a LQ manner, but will emphasise some frequency regions in order to reduce the loads. For that purpose, we introduce some filters in the cost function:

$$\mathbf{x}^{\breve{y}}_{k+1} =\mathbb{A}^{\breve{y}}\mathbf{x}^{\breve{y}}_k + \mathbb{B}^{\breve{y}}\mathbf{y}_k,\ \breve{\mathbf{y}}_k = \mathbb{C}^{\breve{y}}\mathbf{x}^{\breve{y}}_k + D^{\breve{y}}\mathbf{y}_k, \tag{7}$$

$$\mathbf{x}^{\breve{u}}_{k+1} =\mathbb{A}^{\breve{u}}\mathbf{x}^{\breve{u}}_k + \mathbb{B}^{\breve{u}}\mathbf{u}_k,\ \breve{\mathbf{u}}_k = \mathbb{C}^{\breve{u}}\mathbf{x}^{\breve{u}}_k + \mathbb{D}^{\breve{u}}\mathbf{u}_k. \tag{8}$$

At each time step k, knowing the initial conditions $\mathbf{x}_0 = \mathbf{x}_k$, $\mathbf{x}^{\breve{y}}_0 = \mathbf{x}^{\breve{y}}_k$ and $\mathbf{x}^{\breve{u}}_0 = \mathbf{x}^{\breve{u}}_k$, predicting the disturbances $D = \begin{bmatrix}\mathbf{d}'_k & \dots & \mathbf{d}'_{k+N-1}\end{bmatrix}'$ and the inputs $U = \begin{bmatrix}\mathbf{u}'_k & \dots & \mathbf{u}'_{k+N-1}\end{bmatrix}'$ over the horizon length N, the outputs $Y = \begin{bmatrix}\mathbf{y}'_{k+1} & \dots & \mathbf{y}'_{k+N}\end{bmatrix}'$ and the filtered outputs $\breve{Y} = \begin{bmatrix}\breve{\mathbf{y}}'_{k+1} & \dots & \breve{\mathbf{y}}'_{k+N}\end{bmatrix}'$ can be predicted and the filtered inputs $\breve{U} = \begin{bmatrix}\breve{\mathbf{u}}'_{k+1} & \dots & \breve{\mathbf{u}}'_{k+N}\end{bmatrix}'$ can be calculated over the horizon length N:

$$Y =\Phi\mathbf{x}_0 + \Gamma U + \Gamma_d D + \xi \tag{9}$$

$$\breve{Y} =\Phi_{\breve{y}}\mathbf{x}^{\breve{y}}_0 + \Gamma_{\breve{y}} Y + \breve{\xi} \tag{10}$$

$$\breve{U} =\Phi_{\breve{u}}\mathbf{x}^{\breve{u}}_0 + \Gamma_{\breve{u}} U \tag{11}$$

where ξ and $\breve{\xi}$ are zero mean, Gaussian white noise and

$$\Phi = \begin{bmatrix}\mathbb{C}\mathbb{A}\\ \mathbb{C}\mathbb{A}^2\\ \vdots\\ \mathbb{C}\mathbb{A}^N\end{bmatrix}\ \Phi_{\breve{y}} = \begin{bmatrix}\mathbb{C}^{\breve{y}}\\ \mathbb{C}^{\breve{y}}\mathbb{A}^{\breve{y}}\\ \vdots\\ \mathbb{C}^{\breve{y}}\mathbb{A}^{\breve{y}N-1}\end{bmatrix}\ \Phi_{\breve{u}} = \begin{bmatrix}\mathbb{C}^{\breve{u}}\\ \mathbb{C}^{\breve{u}}\mathbb{A}^{\breve{u}}\\ \vdots\\ \mathbb{C}^{\breve{u}}\mathbb{A}^{\breve{u}N-1}\end{bmatrix}$$

$$\Gamma = \begin{bmatrix}\mathbb{C}\mathbb{B} & 0 & \dots & 0\\ \mathbb{C}\mathbb{A}\mathbb{B} & \mathbb{C}\mathbb{B} & & \vdots\\ \vdots & & \ddots & \vdots\\ \mathbb{C}\mathbb{A}^{N-1}\mathbb{B} & \dots & \dots & \mathbb{C}\mathbb{B}\end{bmatrix}$$

Γ_d is defined in a similar way as Γ.

$$\Gamma_{\breve{y}} = \begin{bmatrix}\mathbb{D}_{\breve{y}} & 0 & \dots & 0\\ \mathbb{C}_{\breve{y}}\mathbb{B}_{\breve{y}} & \mathbb{D}_{\breve{y}} & & \vdots\\ \vdots & & \ddots & \vdots\\ \mathbb{C}_{\breve{y}}\mathbb{A}_{\breve{y}}^{N-1}\mathbb{B}_{\breve{y}} & \dots & \mathbb{C}_{\breve{y}}\mathbb{B}_{\breve{y}} & \mathbb{D}_{\breve{y}}\end{bmatrix}$$

and $\Gamma_{\breve{u}}$ is defined in a similar way as $\Gamma_{\breve{y}}$.

C. Cost function and constraints

The purpose of the controller is to decrease the variations of the blade root flap moment with emphasise on some given frequencies. It is important to preserve the actuators as well, by avoiding unnecessary actuations.

The cost function ϕ consists in:

- a cost $\phi_{\breve{y}}$ on the filtered outputs in order to do frequency weighted control on the blade root flap moment
- a cost ϕ_u on the TEF angles
- a cost $\phi_{\breve{u}}$ on the filtered inputs so that actuation of the TEF at high frequencies can be avoided.

$$\begin{aligned}\phi =&\underbrace{\sum_{i=1}^{N}||\breve{y}_i||^2_{W_{\breve{y}}}}_{\phi_{\breve{y}}} + \underbrace{\sum_{i=1}^{N}||u_i||^2_{W_u}}_{\phi_u} + \underbrace{\sum_{i=1}^{N}||\breve{u}_i||^2_{W_{\breve{u}}}}_{\phi_{\breve{u}}}\\ =&\frac{1}{2}\left[\breve{Y}'W_{\breve{Y}}\breve{Y} + U'W_U U + \breve{U}'W_{\breve{U}}\breve{U}\right]\end{aligned} \tag{12}$$

Combining (9), (10), (11) and (12) leads to $\Phi = \frac{1}{2}U'HU + b'U + c$, where

$$\begin{aligned}H =&\Gamma'\Gamma'_{\breve{y}}W_{\breve{Y}}\Gamma_{\breve{y}}\Gamma + W_U + \Gamma'_{\breve{u}}W_{\breve{U}}\Gamma_{\breve{u}y},\\ b =&\Gamma'\Gamma'_{\breve{y}}W_{\breve{Y}}\left(\Phi_{\breve{y}}\mathbf{x}^{\breve{y}}_0 + \Gamma_{\breve{y}}\left(\Phi x_0 + \Gamma_d D\right)\right) + \Gamma'_{\breve{u}}W_{\breve{U}}\Phi_{\breve{u}}\mathbf{x}^{\breve{u}}_0,\end{aligned}$$

and c is a term independent of U. Hard constraints are added on the TEF angles and angle rates.

$$\mathcal{U} := \{U \in [U_{min}, U_{max}], \Delta U \in [\Delta U_{min}, \Delta U_{max}]\},$$

where ΔU is the vector of TEF angles difference $[u_{l+1} - u_l]_{l\in[0;N-1]}$. Extreme flapwise bending moment is not an issue for this controller, so constraints on the states are not necessary.

So, the model predictive control consists in solving, at each time step, the quadratic program $\min_{U\in\mathcal{U}}\left(\frac{1}{2}U'HU + b'U\right)$.

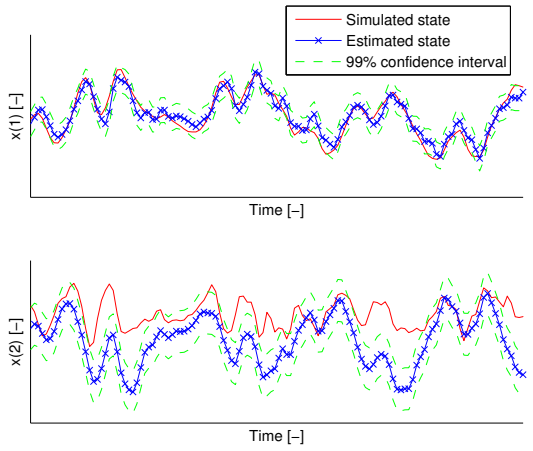

Fig. 2. Estimated (blue) and true (red) states of the system. The 99% confidence interval is indicated in dash green.

D. Kalman filter

Blade deflection and deflection rate are not easy to measure on a turbine. A Kalman filter is necessary to estimate the states. The predictive Kalman filter is prefered over the ordinary filter in order to ease the implementation of the controller in the real turbine.

At each time step k, $\hat{\mathbf{x}}_{k+1|k}$ is the states estimates at the next time step $k+1$, based on the inputs $\mathbf{u}_k$, the disturbances $\mathbf{d}_k$ and the measurements $\mathbf{y}_k$ at time step k.

$$\hat{\mathbf{x}}_{k+1|k} = \left(\mathbb{A}^d - K\mathbb{C}_m^d\right)\hat{\mathbf{x}}_{k|k-1} + \mathbb{B}^d\mathbf{u}_k + \mathbb{G}^d\mathbf{d}_k + K\mathbf{y}_k$$

where $K = \mathbb{A}^d P \mathbb{C}^{d'} \left(\mathbb{C}^d P \mathbb{C}^{d'} + R_2\right)^{-1}$ and P is the solution of the discrete time algebraic Riccati equation $\mathbb{A}^d P \mathbb{A}^{d'} - P - K\mathbb{C}^d P \mathbb{A}^{d'} + R_1 = 0$.

Fig. 2 shows that the first state of the system, proportional to the blade deflection, is well estimated by the predictive Kalman filter and is most of the time within the 99% confidence interval. The second state, proportional to the blade deflection rate, is not predicted as well as the first state because of a plant-model mismatch. Input or output disturbance models are usually used in order to deal with this mismatch and to achieve offset-free MPC [16]. As the objective of this controller is to reduce the variance of the output, those disturbance states are not strictly needed.

E. Gain scheduling

Some non linearities of the system are due to the non-linearity of the lift and drag polars of the blade airfoils. Depending on the free wind speed, the airfoils operates in different regions of their polar curves. Those non-linearities are minimised by using gain scheduling on the average free wind speed inflow V. The model matrices $\mathbb{A}$, $\mathbb{B}$, $\mathbb{C}$, $\mathbb{C}_m$ and $\mathbb{G}$, and therefore Φ, $\Phi_{\breve{y}}$, $\Phi_{\breve{u}}$, Γ, Γ_d, $\Gamma_{\breve{y}}$, $\Gamma_{\breve{u}}$ and K all depend on V. They are calculated offline at several values of V, and they are interpolated online depending on the free wind speed.

Defining the mean free wind speed V is tricky because of the spatial and time turbulence of the wind. Ostergaard et al. designed a wind speed estimator based on the rotor speed, the aerodynamic torque and the pitch angle [17]. The estimated effective wind speed is meant to be used for gain scheduling of their controllers. Instead, the mean free wind speed V seen by the V27 turbine is estimated from a look-up table function of the pitch angle and the flap blade root moment of the 3 blades.

Low pass filters ensures that the estimated effective wind speed is a smooth function of time.

IV. Results

A. Simulation code

Numerical analysis is carried out with the aeroelastic code Flex5, developed by DTU Mechanical Engineering. It is a state-of-the art Blade Element Momentum code based on the modal approach. Both blades and tower are flexible, modeled by as many mode shapes as required. It has all the usual engineering models used in the wind turbine simulation tools, such as Prandtl-Glauert tip correction, dynamic wake model, turbulent wind, oblique inflow model etc. The dynamic stall model originally coded in Flex5 works only for rigid blade sections [18]. The implementation of the trailing edge flaps aerodynamics in Flex5 is based on the model written by Andersen et al. [14]. Flex5 has a fixed-step solver; a frequency of 50 Hz is used in those simulations.

Notice that the simulation model Flex5 differs significantly from the design model (2). The simulation model takes into account the induced velocities lags, the aerodynamic lags and the elasticity of all the turbine components. The blade is no longer modeled by its first mode only, but by its three first modes. The pitch is actuated in order to regulate the produced power, and the rotor speed is no longer strictly constant. The Flex5 code has been used for a long time, and its results match reasonably the measurements made on real turbines.

The open source code qpOASES [19][20] is used to solve the quadratic program, real-time, at 50 Hz.

B. Blade root flap moment spectral density

Fig. 3 shows the typical spectral density of the flapwise blade root moment when the turbine is in normal production. The 1P frequency corresponds to one event per rotor revolution, the 2P and 3P frequencies are the double and the triple of the 1P frequency. Loads at those frequencies are consequences of events such as tower shadow, wind shear or yaw misalignment. Loads can also be seen at the first flapwise and the first edgewise eigenfrequencies of the blade. Those modes are usually well damped, either by the structural damping of the blade or by the aerodynamic damping.

Fatigue damage of the blade root depends on the number of load cycles the blade is going through, but also on the amplitude of those cycles. Loads at frequencies 1P, 2P and 3P are the most important loads regarding fatigue damage of the blade.

C. Frequency weighted control of the blade root moment

The model predictive control described in this paper is designed in order to alleviate loads at given frequencies. This is done by tuning the filter on the outputs (7). A Butterworth bandpass filter of low order is used to decrease the loads at frequencies between the cut-in and the cut-out frequencies. The purpose of the controller is not to reduce the mean blade root flap moment, so the steady-state gain of the filter has to be 0.

In a first time, 3 bandpass filters are designed so that the controllers MPC 1, MPC 2 and MPC 3 alleviate respectively the 1P, 2P and 3P loads. Simulations are run with Flex5 with those 3 controllers, with exactly the same wind conditions. Fig. 3 shows the spectral densities of the blade root flap moment and of one of the 3 TEF angle. The 3 controllers manage to reduce the loads within the frequency range they have been designed for, MPC 1 being the best to reduce the 1P loads, MPC 2 the 2P loads and MPC 3 the 3P loads. Each of those 3 controllers reduce loads at frequencies between 1P and 3P. But, on the other hand, they increase the amplitude of the loads at frequencies higher than 3P: those high frequency, high amplitude loads damage a lot the materials. This wrong behavior of the controller is a consequence of a plant-model mismatch. The model does not include a dynamic model of the aero forces around the airfoil. At high actuation frequencies, the time lag between the TEF position and the change in lift coefficient can no longer be neglected, and the fact that it is not included in the design model of the MPC may end up in those extra loads.

This mismatch can be minimised by fine tuning the Kalman filter, and increasing the variance on the measurement noise ν. Two new controllers, MPC 4 and MPC 5, are designed in order to alleviate the loads at frequencies between 1P and 3P. The Kalman filter of MPC 4 is the same as the one used in MPC 1 to MPC 3. In MPC 5, the Kalman filter is tuned in order to avoid the extra loads at frequencies higher than 3P. Fig. 4 shows that MPC 5 is as good as MPC 4 to alleviate loads at frequencies between 1P and 3P, and, at the same time, it does no longer increase the loads at frequencies close to 4P.

A last improvement of the MPC consists in decreasing the TEF activity at high frequencies, where they do not help reducing the blade root loads, but where they wear out the actuator systems. The filter on the inputs (8) is used for this purpose: a Butterworth high pass filter is designed in order to emphasise the cost on the high frequency trailing edge flaps actuation. MPC 6 is similar to MPC 5, but with this extra cost on the high pass filtered inputs. Figure 5 shows the results of simulations made with these controllers: the blade root loads with controllers MPC 5 and MPC 6 are similar over the whole spectrum, but actuators controlled by MPC 6 have a much lower activity at high frequencies. The damage of the blade root is unchanged, while the fatigue damage of the actuator system is decreased.

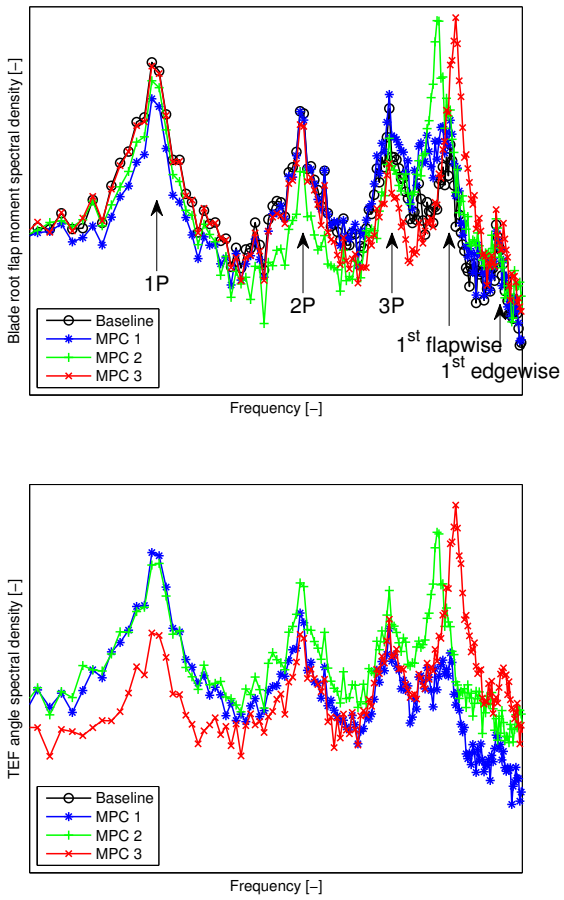

Fig. 3. Blade root flap moment (top) and trailing edge flaps angle (bottom) spectral density when TEF are not actuated (baseline test) and when controllers MPC 1, MPC 2 or MPC 3 are used to control the TEF. Those controllers aim at alleviating the blade root flap moment at respectively the 1P, 2P and 3P frequencies.

V. Conclusion

A model predictive control has been designed in order to alleviate blade root loads with emphasize on given load frequencies. This controller, while used with the Flex5 simulation code, shows its ability to focus on fixed frequencies. The tuning of the Kalman filter and of the inputs filter are essential in order to reach a good trade off between blade damage and actuator damage. Robustness and stability will have to be tested before testing on the V27 turbine at Risø DTU, National Laboratories for Sustainable Energy.

References

[1] T. J. Larsen, H. A. Madsen, and K. Thomsen, "Active load reduction using individual pitch, based on local blade flow measurements," *Wind Energy*, vol. 8, no. 1, pp. 67–80, 2005.

[2] E. A. Bossanyi, "Individual blade pitch control for load reduction," *Wind Energy*, vol. 6, pp. 229–244, 2003.

[3] T. Barlas and G. van Kuik, "Review of state of the art in smart rotor control research for wind turbines." *Prog Aerospace Sci*, 2009.

[4] T. Buhl, M. Gaunaa, and C. Bak, "Potential load reduction using airfoils with variable trailing edge geometry," *Journal of Solar Energy Engineering*, vol. 127, pp. 503–516, November 2005.

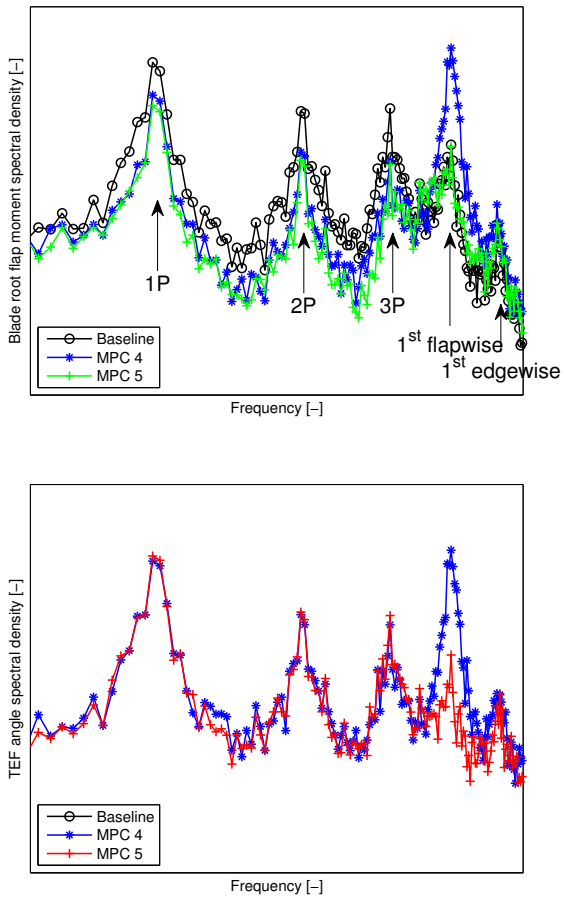

Fig. 4. Blade root flap moment (top) and trailing edge flap angle (bottom) spectral density when TEF are not actuated (baseline test) and when controllers MPC 4 or MPC 5 are used. Those controllers aim at alleviating the blade root flap moment at frequencies up to 3P. The Kalman filter used in the controller MPC 5 is tuned in order to avoid extra loads at frequencies higher than 4P.

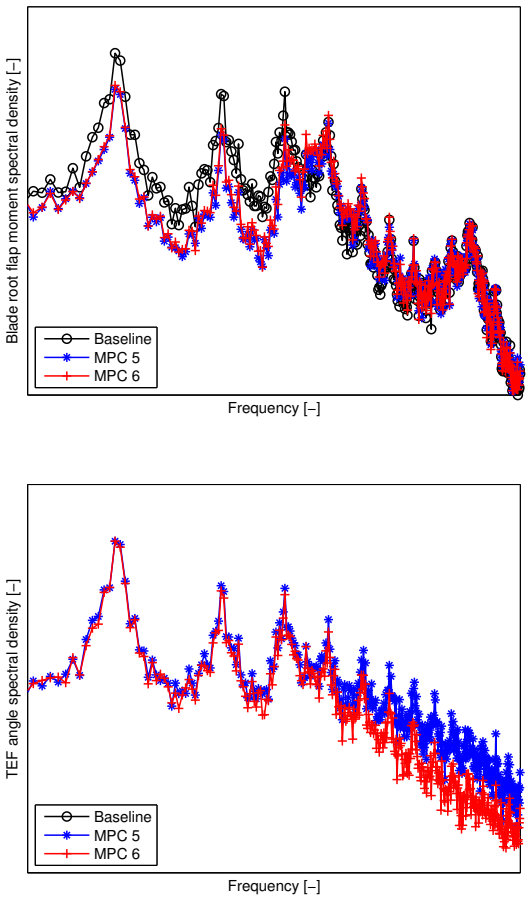

Fig. 5. Blade root flap moment (top) and trailing edge flap angle (bottom) spectral density when TEF are not actuated (baseline test) and when controllers MPC 5 or MPC 6 are used. Those controllers aim at alleviating the blade root flap moment at frequencies up to 3P. A cost on the high pass filtered inputs is added in MPC 6, resulting in a decrease of the actuator activity at high frequencies, without decreasing the controller efficiency.

[5] P. B. Andersen, M. Gaunaa, C. Bak, and T. Buhl, "Deformable trailing edge flaps for modern megawatt wind turbine controllers using strain gauge sensors," *Wind Energy*, vol. 13, no. 2, pp. 193–206, 2010.

[6] C. Bak, M. Gaunaa, P. B. Andersen, T. Buhl, P. Hansen, and K. Clemmensen, "Wind tunnel test on airfoil Risø-b1-18 with an active trailing edge flap," *Wind Energy*, vol. 13, no. 2-3, pp. 207–219, 2010.

[7] J. W. van Wingerden, A. W. Hulskamp, T. Barlas, B. Marrant, G. A. M. van Kuik, D.-P. Molenaar, and M. Verhaegen, "On the proof of concept of a 'smart' wind turbine rotor blade for load alleviation," *Wind Energy*, vol. 11, pp. 265–280, 2008.

[8] J. W. van Wingerden, A. Hulskamp, T. Barlas, I. Houtzager, H. Bersee, G. van Kuik, and M. Verhaegen, "Two-degree-of-freedom active vibration control of a prototyped smart rotor," *IEEE Transactions on Control Systems Technology*, vol. 19, no. 2, pp. 284–296, 2011.

[9] D. Castaignet, J. J. Wedel-Heinen, T. Kim, T. Buhl, and N. K. Poulsen, "Results from the first full scale wind turbine equipped with trailing edge flaps." Chicago, Illinois: 28th AIAA Applied Aerodynamics Conference, June 2010.

[10] M. Lackner and G. van Kuik, "A comparison of smart rotor control approaches using trailing edge flaps and individual pitch control," *Wind Energy*, vol. 13, pp. 117–134, 2010.

[11] J. K. Rice and M. Verhaegen, "Robust and distributed control of a smart blade," *Wind Energy*, vol. 1, pp. 103–116, 2010.

[12] D. G. Wilson, D. E. Berg, M. F. Barone, J. C. Berg, B. R. Resor, and D. W. Lobitz, "Active aerodynamic blade control design for load reduction on large wind turbines." Marseille, France: European Wind Energy Conference & Exhibition, March 2009.

[13] M. O. L. Hansen, *Aerodynamics of Wind Turbines*. Earthscan, 2008.

[14] P. B. Andersen, M. Gaunaa, C. Bak, and M. H. Hansen, "A dynamic stall model for airfoils with deformable trailing edges," *Wind Energy*, vol. 12, no. 8, pp. 734–751, 2009.

[15] K. Hammerum, P. Brath, and N. K. Poulsen, "A fatigue approach to wind turbine control," *Journal of Physics: Conference Series*, vol. 75, no. 1, 2007.

[16] G. Pannocchia and J. B. Rawlings, "Disturbance models for offset-free model-predictive control," *AIChE Journal*, vol. 49, no. 2, pp. 426–437, 2003.

[17] K. Z. Ostergaard, P. Brath, and J. Stoustrup, "Estimation of effective wind speed," *Journal of Physics: Conference Series*, vol. 75, no. 1, 2007.

[18] S. Øye, "Dynamic stall simulated as time lag of separation." Thessaloniki, Greece: European Wind Energy Conference EWEC, October 1994.

[19] qpOASES homepage. [Online]. Available: http://www.kuleuven.be/optec/software/qpOASES

[20] H. Ferreau, H. Bock, and M. Diehl, "An online active set strategy to overcome the limitations of explicit mpc," *International Journal of Robust and Nonlinear Control*, vol. 18, no. 8, pp. 816–830, 2008.